

Error model development for ARAIM exploiting satellite motion

Elisa Gallon, *Illinois Institute of Technology*

Mathieu Joerger, *Virginia Tech*

Santiago Perea, *Airbus Defence and Space GmbH, Munich, Germany*

Boris Pervan, *Illinois Institute of Technology*

BIOGRAPHIES

Elisa Gallon received her Bachelor's Degree in Mathematics from Université Blaise Pascal, France in 2014 and her Master of Science in Global Navigation Satellite Systems from ENAC and ISAE-Supaéro in 2016. From 2016 to 2017, she worked at the European Space Agency (ESA) on Orbit Determination and Time Synchronization of Galileo satellites. She is currently a Ph.D. Candidate at the Navigation Laboratory in the Department of Mechanical and Aerospace Engineering at Illinois Institute of Technology (IIT) in Chicago.

Dr. Mathieu Joerger obtained a Master in Mechatronics from the National Institute of Applied Sciences in Strasbourg, France, in 2002. He earned a M.S. in 2002 and a Ph.D. in 2009 in Mechanical and Aerospace Engineering at IIT in Chicago. He is the 2009 recipient of the Institute of Navigation (ION) Bradford Parkinson award, and the 2014 recipient of the ION Early Achievement Award. He is also an Associate Editor of Navigation for the Institute of Electrical and Electronics Engineers (IEEE) Transactions on Aerospace and Electronic Systems. Dr. Joerger is currently assistant professor at Virginia Tech, in Blacksburg, VA, working on multi-sensor integration for safe navigation and collision warning of automated driving systems (ADS). He is a member of the E.U./U.S. Advanced RAIM (ARAIM) Working Group C.

Dr. Santiago Perea obtained a Master of Science in Aerospace Engineering from University of Sevilla (Spain) in 2013. In parallel, as a double degree student, he gained his Master in Mechanical and Aerospace Engineering from Illinois Institute of Technology (Chicago). He earned his Ph.D. in Electrical Engineering from RWTH Aachen University (Germany) in 2019. From 2013 to 2018 he was a research associate at the Institute of Communications and Navigation at German Aerospace Center (DLR). In June 2018 he joined the GNSS Performance Team at Airbus Defence & Space in Munich, Germany. His current research includes GNSS performance and integrity with a particular focus on Advanced Receiver Autonomous Integrity Monitoring (ARAIM).

Dr. Boris Pervan is a Professor of Mechanical and Aerospace Engineering at IIT, where he conducts research on advanced navigation systems. Prior to joining the faculty at IIT, he was a spacecraft mission analyst at Hughes Aircraft Company (now Boeing) and a postdoctoral research associate at Stanford University. Prof. Pervan received his B.S. from the University of Notre Dame, M.S. from the California Institute of Technology, and Ph.D. from Stanford University. He is an Associate Fellow of the AIAA, a Fellow of the Institute of Navigation (ION), and Editor-in-Chief of the ION journal NAVIGATION. He was the recipient of the IIT Sigma Xi Excellence in University Research Award (2011, 2002), Ralph Barnett Mechanical and Aerospace Dept. Outstanding Teaching Award (2009, 2002), Mechanical and Aerospace Dept. Excellence in Research Award (2007), University Excellence in Teaching Award (2005), IEEE Aerospace and Electronic Systems Society M. Barry Carlton Award (1999), RTCA William E. Jackson Award (1996), Guggenheim Fellowship (Caltech 1987), and Albert J. Zahm Prize in Aeronautics (Notre Dame 1986).

ABSTRACT

In this paper, we derive new satellite orbit and clock error models for time sequential, dual frequency, multi-constellation Advanced Receiver Autonomous Integrity Monitoring (ARAIM). In the current implementation of baseline 'snapshot' ARAIM, Carrier Smoothed Code (CSC) measurements at one instant in time are used to provide a navigation solution. Using a time-sequential implementation of ARAIM, i.e., using measurements collected over time, will significantly reduce Protection Levels (PL). It was shown in [3] that snapshot ARAIM cannot provide better performance than LPV-200, which has a 35 m Alert Limit (AL). Exploiting satellite motion will lead to superior positioning performance and significantly tighter PLs relative

to baseline snapshot ARAIM, possibly even achieving 10 m ALs to support Category II aircraft approaches. In order to implement this time sequential approach, orbit and clock errors need to be characterized over time. In this paper, we process GPS and Galileo orbit and clock data to evaluate and analyze ranging errors over time. We then determine upper and lower bounds on ranging errors autocorrelation functions. These bounds will be implemented to over-bound time-sequential positioning errors.

INTRODUCTION

Receiver Autonomous Integrity Monitoring (RAIM) uses redundant measurements to detect faults. RAIM was initially intended to support horizontal guidance for aircraft during en-route flights using GPS L1 only. But with the development of GLONASS, Galileo and Beidou, the number of available measurements has increased. In addition, the provision of dual-frequency signals allows for removal of ionospheric delay, which was the largest source of ranging error. In consequence, extensive efforts have been made to develop a new dual frequency, multi-constellation Advanced RAIM (ARAIM) fault detection and exclusion (FDE) method. ARAIM is now intended to support applications such as vertical guidance. Reference [3] describes optimal estimators and detectors that minimize the integrity risk in ARAIM and identifies the circumstances under which dual-frequency GPS/Galileo satisfies requirements for localizer performance with vertical guidance down to 200 feet above the runway (LPV-200).

In the current implementation of baseline ARAIM, carrier smoothed code (CSC) measurements from multiple satellites are combined at one time-instant to obtain a position estimate and perform fault detection. By using CSC measurements, snapshot ARAIM exploits code noise averaging against the carrier using Hatch filters. However, it was shown in [3] that when nominal constellations are depleted, LPV-200 could only be sparsely achieved. Further, snapshot ARAIM cannot provide better performance than LPV-200 even under optimistic constellation assumptions.

To address this issue, a time-sequential ‘batch’ implementation of ARAIM was presented in [1]. Several versions of the batch implementation have been studied. Initially, raw code and carrier measurements were collected at a one-Hertz rate over a fixed time interval (e.g., 10 min), and processed in a sliding window batch estimator. The method was computationally expensive, but the results obtained in [1] showed a significant reduction in probability of hazardously misleading information P_{HMI} when using batch ARAIM compared to snapshot ARAIM.

In [1], we also presented a computationally efficient batch ARAIM which used CSC measurements taken at a few, infrequent sample times (e.g. every 5 min). The use of CSC retains the existing benefits in baseline ARAIM by averaging out code phase noise and multipath over time using Hatch filters. The additional use of carrier measurements obtained at temporally-separated epochs provides observability of floating cycle ambiguities from a completely different, complementary source: satellite geometry change. An extra advantage of this CSC-based approach is that the batch ARAIM becomes a straightforward augmentation of snapshot ARAIM, and the FDE function only requires minor adjustments.

One major challenge in batch ARAIM is that measurement errors must be modeled over time. In [1], we made assumptions on these models that must be validated with data. In addition, if the measurement error time-correlation function cannot be determined with high certainty, we need to account for our lack of knowledge on error dynamics over time. Reference [11] describes a method to obtain guaranteed bounds on positioning errors for batch estimators using measurements with unknown but bounded time correlation functions.

In this paper, we describe new measurement error models over time, including upper and lower bounds on the error autocorrelation functions derived from data. The paper focuses on the main driver of range error: orbit and clock errors.

MEASUREMENT ERROR MODEL

The batch implementation chosen in this paper uses CSC and carrier phase measurements taken at $K = T_{RBS}/T_S$ sample times (where T_{RBS} is the batch sample spacing, and T_S is the receiver sampling time). In [1], the measurement model, which we will refine based on our data analysis, is expressed as:

$$\begin{bmatrix} \bar{\rho} \\ \bar{\phi} \end{bmatrix} = \begin{bmatrix} G & \mathbf{0} & H_{ERR} \\ G & H_\eta & H_{ERR} \end{bmatrix} \begin{bmatrix} \mathbf{u} \\ \eta \\ \mathbf{s}_{ERR} \end{bmatrix} + \begin{bmatrix} \mathbf{v}_{T,E,RNMP,\bar{\rho}} \\ \mathbf{v}_{T,E,RNMP,\bar{\phi}} \end{bmatrix} + \begin{bmatrix} \mathbf{b}_\rho \\ \mathbf{b}_\phi \end{bmatrix} \quad (1)$$

where

- $\bar{\rho}$ is the vector of carrier smoothed code $\bar{\rho} = [\bar{\rho}_1 \quad \dots \quad \bar{\rho}_k]^T$
- ϕ is the vector of raw carrier phase measurements $\phi = [\phi_1 \quad \dots \quad \phi_k]^T$
- G is the batch geometry matrix
- η is the vector of constant cycle ambiguities
- \mathbf{u} is the batch position vector: $\mathbf{u} = [\mathbf{u}_1 \quad \dots \quad \mathbf{u}_k]^T$, $\mathbf{u}_k = [X_k^T \quad \tau_{GPS,k} \quad \tau_{GAL,k}]^T$
- \mathbf{s}_{ERR} is a vector of constant error states $\mathbf{s}_{ERR} = [\mathbf{b}_E \quad \mathbf{g}_E]^T$
- $\mathbf{v}_{T,E,RNMP,\bar{\rho}/\phi}$ is the measurement noise vector
- \mathbf{H}_{ERR} is the error state coefficient matrix
- \mathbf{H}_η is the cycle ambiguity coefficient matrix

In the current implementation of ARAIM, the impact of satellite orbit and clock errors on range measurements at the worst user location are characterized by the User Ranging Accuracy (URA). The URA is a high-integrity per-satellite error model defined as a zero mean gaussian distribution with over-bounding standard deviation σ_{URA} . To model errors over time, a ‘bias-plus-ramp’ model was derived in [1]. It can be expressed as:

$${}^i\epsilon_{E,k} = {}^i b_E + {}^i g_E(t_k - t_1) + {}^i \epsilon_{RES,k} \quad (2)$$

where

- ${}^i b_E$ is an unknown constant bias
- ${}^i g_E$ is an unknown constant gradient
- t_1 is the first epoch of the batch interval
- t_k is the k-th epoch within the batch interval, such that $1 \leq k \leq q$, where q is the last epoch of the batch interval
- ${}^i \epsilon_{RES,k}$ are the residual errors

This model has the advantage of being straightforward to incorporate in a batch implementation. However, it was developed for a 10 min batch and won’t necessarily be valid if we wish to extend the batch duration. The next section characterizes orbit and clock errors over time to validate or improve this bias-plus-ramp model. The next section’s approach can be applied to other error sources as well, however to limit the length of this paper, and since satellite orbit and clock error is the main driver of range error, we will focus on orbit and clock errors.

ORBIT AND CLOCKS ERROR CHARACTERIZATION OVER TIME

This section analyses the behavior of orbit and clock errors over time for the GPS and Galileo constellations. Orbit and clock errors are analyzed by differencing of precise, reference orbit and clock measurements with broadcast navigation data. Data files are obtained from the Multi-GNSS EXperiment (MGEX) repositories. The following two sub-sections describe these inputs.

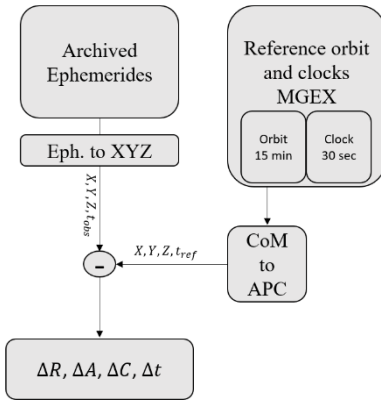


Figure 1: Error generation

Reference orbit and clocks

MGEX was initiated by the International GNSS Service (IGS) with the goal of creating one GNSS data service for multiple constellations. It is comprised of Analysis Centers (AC) which compute their own GNSS products. In this work, we use precise orbit data from two ACs: CODE for GPS and CNES for Galileo and will consider it our reference (see repository [9]). These files contain orbit and clock data at a 15 min sampling rate. Since we are interested in characterizing orbit and clock errors over a short period of time (several hours), getting data every 15 min will not suit us, and we will need to interpolate the data. In this paper we use an 8th order Lagrange polynomial (according to the analysis from Ref [15]). Clocks perform as random walk processes and should not be interpolated. Instead, we will use the clock products from IGS provided at a 30s sampling rate. It is important to note that these orbit data are provided with respect to satellite center of mass and we will convert them to describe the motion of the phase center, following the procedure used in [10], to be consistent with the broadcast ephemerides.

Broadcast ephemerides

Broadcast ephemerides are stored in Receiver Independent Exchange (RINEX) formats that contain 24 hours of navigation message. This work makes use of Stanford University ‘sugl’ files for GPS satellites and ‘brdc’ from CNES for Galileo (see repositories [7] and [8]). Those institutions were chosen among several others for their cleaning and validation algorithms ensuring a limited amount of file recording, storing and labeling issues.

Orbit and clock error autocorrelation

Satellite orbit and clock error are obtained by comparing the satellite orbit and clock derived from the broadcast ephemerides to the reference orbits (as shown in Figure 1). They are expressed in satellite’s reference body frame Radial, Along-track and Cross-track. Note that reference orbits are provided with respect to center of mass (CoM) of the satellite, whereas broadcast ephemerides are decoded with respect to the satellite’s antenna phase center (APC). This offset is provided in the ANTenna EXchange (ANTEX) files for each GPS and Galileo satellites (see APC conventions for MGEX at Ref [14]). After correcting for that offset, orbit and clock errors are obtained by differencing reference and broadcast orbit and clocks. Figure 2 represents the time evolution of the GPS and Galileo satellites (each color represents a satellite), in terms of radial plus clock errors for a chosen date (1st of December 2018).

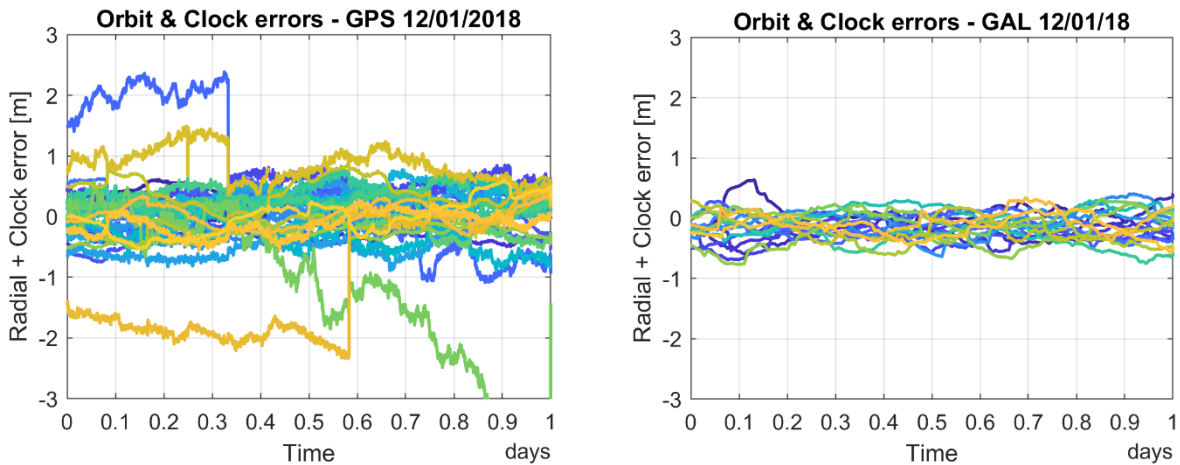


Figure 2: Time evolution of Radial Plus Clock errors for GPS (left) and Galileo (right) satellites on 12/10/2018

Note that the ephemerides are broadcast every 2 hours. When a new set of ephemerides is received, the old one is still valid for two more hours (for GPS), although most users will decide to use the new set as soon as they receive it. This new upload creates a ‘jump’ in the estimated satellites positions. To account for this effect, the broadcast ephemerides from the current and following sets of ephemerides were interpolated in the position domain through weights over two hours (see Appendix A).

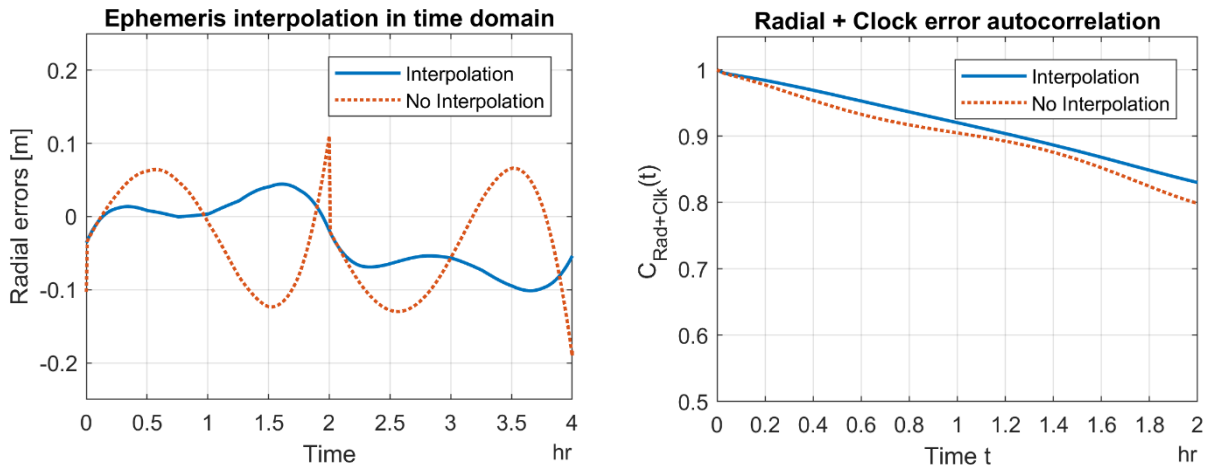


Figure 3: Interpolation of ephemeris jumps (left) and their impact on error autocorrelation (right)

Figure 3 (left) represents the radial error of GPS PRN 07 before and after interpolation of the ephemerides, with a visible ephemeris jump at 2h. The figure on the right represents the normalized autocorrelation of radial plus clock errors with and without interpolation. The interpolation of ephemerides has a negligible impact on the orbit and clock errors autocorrelation. However, the purpose of this work is to establish a model for orbit and clock errors accounting for their correlation over time, that would be implementable in a batch or Kalman Filter (KF) algorithm. If we did not interpolate those ephemerides jumps, we would have to model their dynamic behavior and input this model to our batch or KF algorithm. Since smoother dynamics are more convenient to model and since we want to model those errors as first order Gauss Markov Process (smooth process), we will use interpolated broadcast ephemerides in this work.

For any random process X , let us define the autocorrelation function R_{XX} of X as:

$$R_{XX}(\xi) = E[X(t)X(t + \xi)] \quad (3)$$

Reference [10] determined bounds on the variance of orbit and clock errors. However, the purpose of this work is to study the time behavior of the orbit and clock errors relative to some current time, because current-time positioning is of main interest in ARAIM. For the rest of this work, when talking about autocorrelation function, we will be referring to its normalized version:

$$C_{XX}(t) = \frac{R_{XX}(t)}{R_{XX}(0)} \quad (4)$$

When dealing with autocorrelation function, a recurrent dilemma arises between stationarity and autocorrelation estimate accuracy. If we use too few data, the autocorrelation will most likely not be accurate (in part due to the zero padding of the `xcorr` Matlab function), but if we use too much data (very long periods), the process may not be stationary anymore. Reference [12] developed the following expression for the variance of autocorrelation estimate \hat{R}_{XX} for a random process X :

$$\sigma_{\hat{R}_{XX}(t)}^2 = Var[\hat{R}_{XX}(t)] = \frac{1}{T} \int_{-\infty}^{\infty} \hat{R}_{XX}^2(\xi) + \hat{R}_{XX}(\xi + t)\hat{R}_{XX}(\xi - t)d\xi \quad (5)$$

Where

T is the length of data used to estimate R_{XX}

To derive Equation (5), we express the autocorrelation function of radial plus clock errors as a first order Gauss Markov Random Process (GMRP) with the following autocorrelation:

$$\hat{R}_{XX}(t) = \sigma_X^2 e^{-|t|/\tau} \quad (6)$$

Where

τ is the time constant of the GMRP
 σ_X^2 is the variance of the random process X

Substituting (6) into (5) yields:

$$\sigma_{\hat{R}_{XX}(t)}^2 = \left(\frac{\tau}{T} + \left(\frac{\tau + 2t}{T} \right) e^{-\frac{2t}{\tau}} \right) \sigma_X^2 \quad (7)$$

Figure 4 (left) represents the autocorrelation of radial plus clock errors using 4 days of data for each of the GPS satellites (each color ranging from yellow to blue represents one GPS satellite). For our application into ARAIM, we will be looking at time intervals smaller than 2 hours. Therefore, we zoom in on the first 2 hours of the 4 day-long autocorrelation curves. Once again, each curve with color ranging from blue to yellow represents one GPS satellite. From Figure 4 (left), we estimate $\tau = 8$ hours.

Note that the goal of this paper is to bound the normalized autocorrelations of orbit and clock errors. Let us decompose as \hat{R}_{XX} :

$$\hat{R}_{XX}(t) = R_{XX}(t) + \delta R_{XX}(t) \quad (8)$$

Where

$R_{XX}(t)$ is assumed known
 $\delta R_{XX}(t)$ is unknown

Equation (9) describes the variance of the normalized autocorrelation estimate \hat{C}_{XX} (details of the derivations can be found in Appendix B):

$$\sigma_{C_{XX}}^2 = \text{Var}[\hat{C}_{XX}(\tau) - C_{XX}(\tau)] = \frac{\sigma_{R_{XX}(t)}^2}{R_{XX}(0)^2} - \frac{2C_{XX}(t)}{R_{XX}(0)^2} E[\delta R_{XX}(t)\delta R_{XX}(0)] + \frac{C_{XX}(t)^2}{R_{XX}(0)^2} \sigma_{R_{XX}(0)}^2 \quad (9)$$

The second term of Equation (9) is unknown but can be lower bounded by $\sigma_{R_{XX}(0)}^2$ and upper bounded by $\sigma_{R_{XX}(t)}^2$. Therefore, assuming $E[\delta R_{XX}(t)\delta R_{XX}(0)]$ is an average of those two bounds, and substituting (8) for R_{XX} into (9) yields:

$$\sigma_{C_{XX}}^2 = \left(1 - e^{-\frac{|t|}{\tau}}\right) \left(1 + \left(\frac{2t}{T} - 1\right) e^{-2t/\tau}\right) \frac{\tau}{T} \quad (10)$$

Figure 4 (right) represents the results obtained from Equation (10) for different length of data. At 2 hours, the standard deviation of variance of normalized autocorrelation estimate for four days of data is close to 0.08, whereas the one-month result shows a standard deviation of 0.03. These values will be of interest in the following error stationarity analysis, to determine whether the changes observed are due to a lack of accuracy in the estimation of the autocorrelation functions, or if they are due to a non-stationary process.

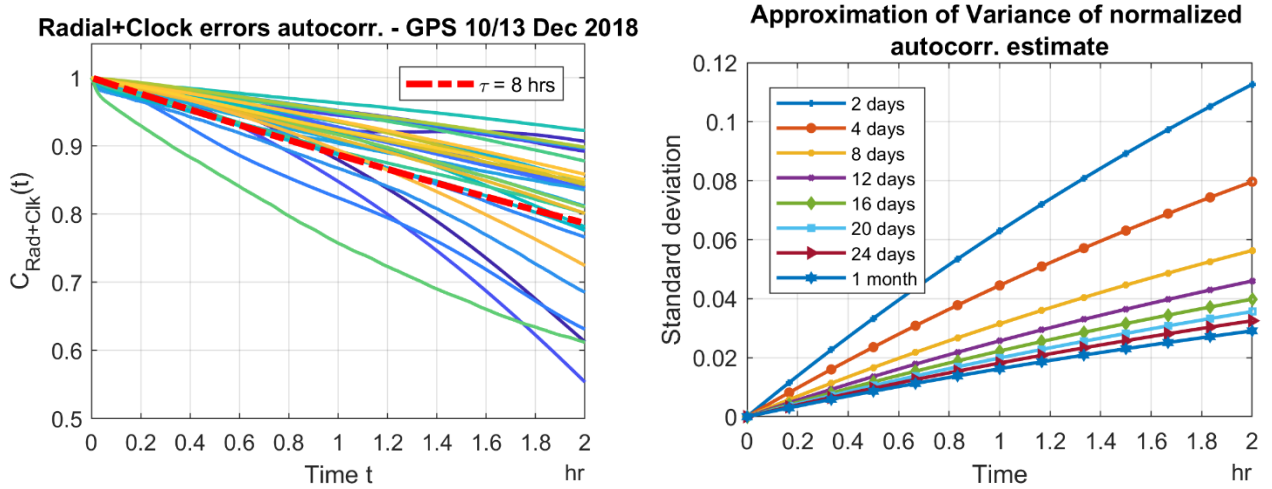


Figure 4: Variance of Autocorrelation Estimate for different length of data

Orbit and clock error stationarity analysis

In the following, we would ideally like to use one month of data to characterize orbit and clock error. By doing so, we obtain a statistical characterization of the orbit and clock errors over time. To use it in our batch implementation, we need to make sure that those statistical properties do not vary (e.g. seasonal changes, lunar cycles) over time. The following paragraphs analyze orbit and clock errors stationarity with respect to lunar cycle, and sun cycle (seasons).

Let us first assess whether orbit and clock errors are stationary over 2 weeks of data. In particular, let us look at the impact of lunar cycles (28 days) on orbit and clock errors. Figure 5 (left) represents the orbit and clock errors autocorrelation obtained with 2 weeks of data for several GPS satellites. For clarity purposes, only 3 satellites of each constellation are shown in these figures (PRN 01, 14 and 31). Full moon occurred on September 24th 2018 and a new moon occurred on September 9th 2018. Therefore, the solid lines represent data from 2nd to 15th of September (new moon) and the dashed lines represent data from 16th to 29th of September (full moon). Looking at these figures and comparing them with the results shown in Figure 4 (right). Figure 5 shows that the lunar cycle has a negligible impact on the orbit and clock errors stationarity of either GPS or Galileo satellites. Indeed, with Figure 4 (right), we concluded that the approximate standard deviation on the autocorrelation estimate was of 0.04 for 2 weeks (i.e. 2 sigma of 0.08), which means that most of the spread we observe on Figure 5 is due to this uncertainty. Therefore, lunar cycles have a negligible effect on orbit and clock errors stationarity. In other words, we can use two weeks of data to bound the autocorrelation of orbit and clock errors. One can notice that satellite E30 has more changes

between the two data sets. These changes seem to be satellite related (presumably clocks) are most likely not due to lunar effects. Further work will need to be performed to assess whether or not these are related to the clocks.

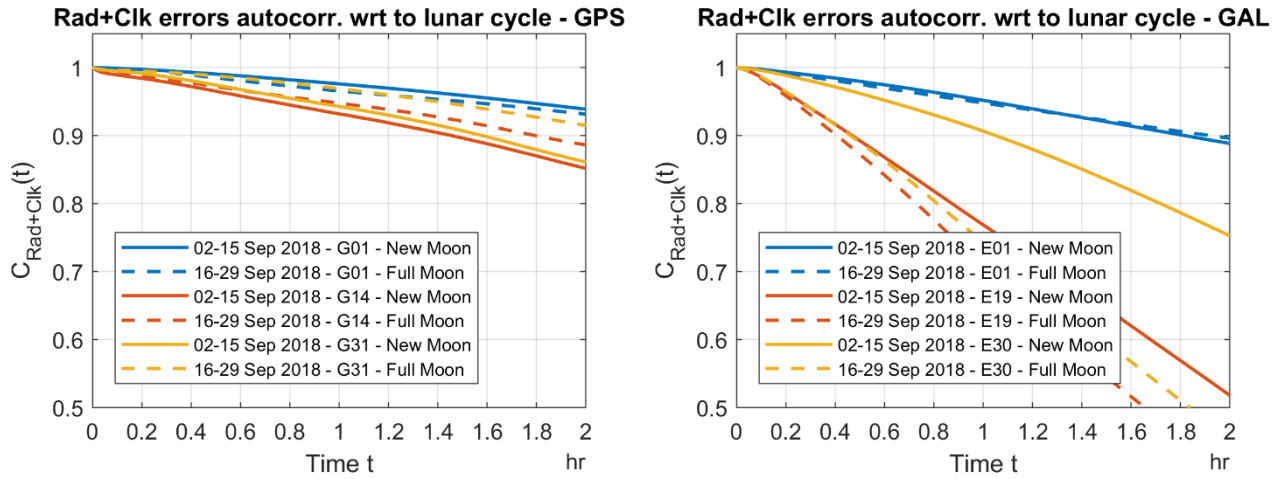


Figure 5: Lunar Cycle impact on orbit and clock errors stationarity of several GPS and Galileo satellites

Let us now look at the impact of seasonal changes on orbit and clock error stationarity. Figure 6 represents the orbit and clock error autocorrelations of each GPS satellite (each color represents one satellite) at 4 different times of the year, using 1 month of data. Once again, each colored curve represents one GPS satellite. The two plots on the left (March and September 2018) are the equinox dates, whereas the two plots on the right (June and December 2018) are the solstice dates. The solstice plots seem to spread slightly wider after 1h, compared to the equinox plots. In Figure 6, the overall behavior (spread) of the GPS autocorrelations, does not vary too much throughout the year. However, if we look satellite-by-satellite, we see that each month is different. Therefore, these results suggest that the orbit and clock errors stationarity may be impacted by the sun cycles (seasons).

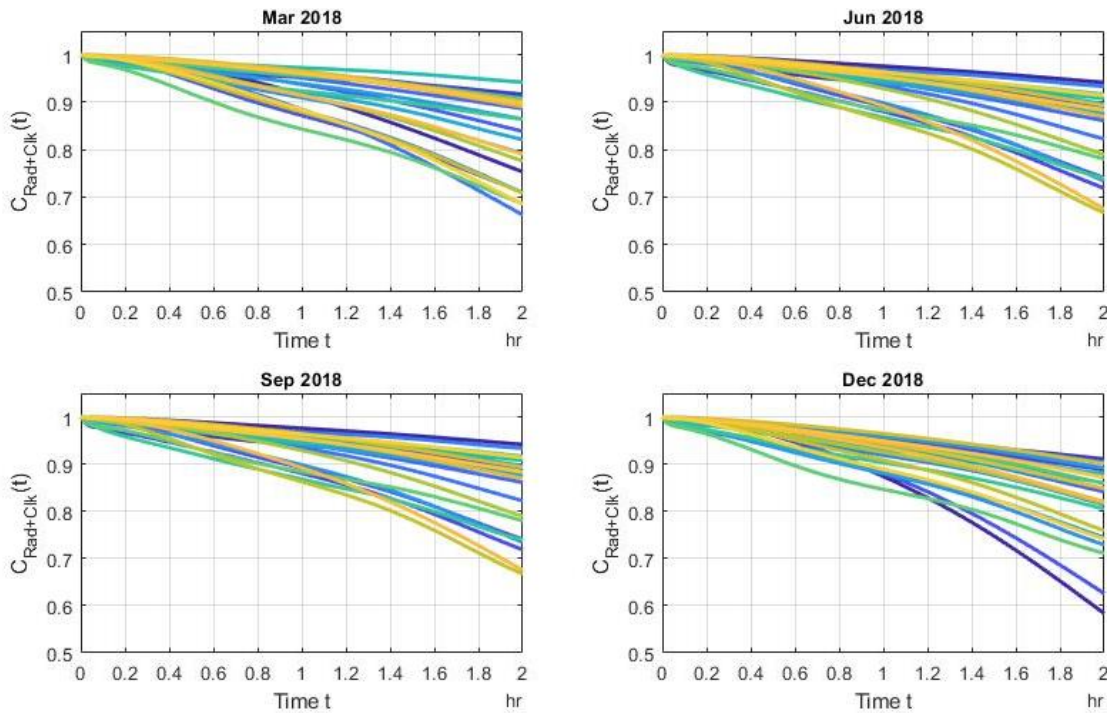


Figure 6: Season impact on orbit and clock errors stationarity of GPS satellites

Similar for Galileo satellites, Figure 7 shows the general trend (i.e. looking at the whole constellation) of orbit and clock errors autocorrelation. Looking at each satellite one-by-one, we notice differences between curves. Certain level of degradation in the orbit error was observed during the month of March. It can possibly be due the less frequent update of the navigation message (nominally 8-12 min) forcing the algorithm to extend the use of broadcast ephemeris for longer periods.

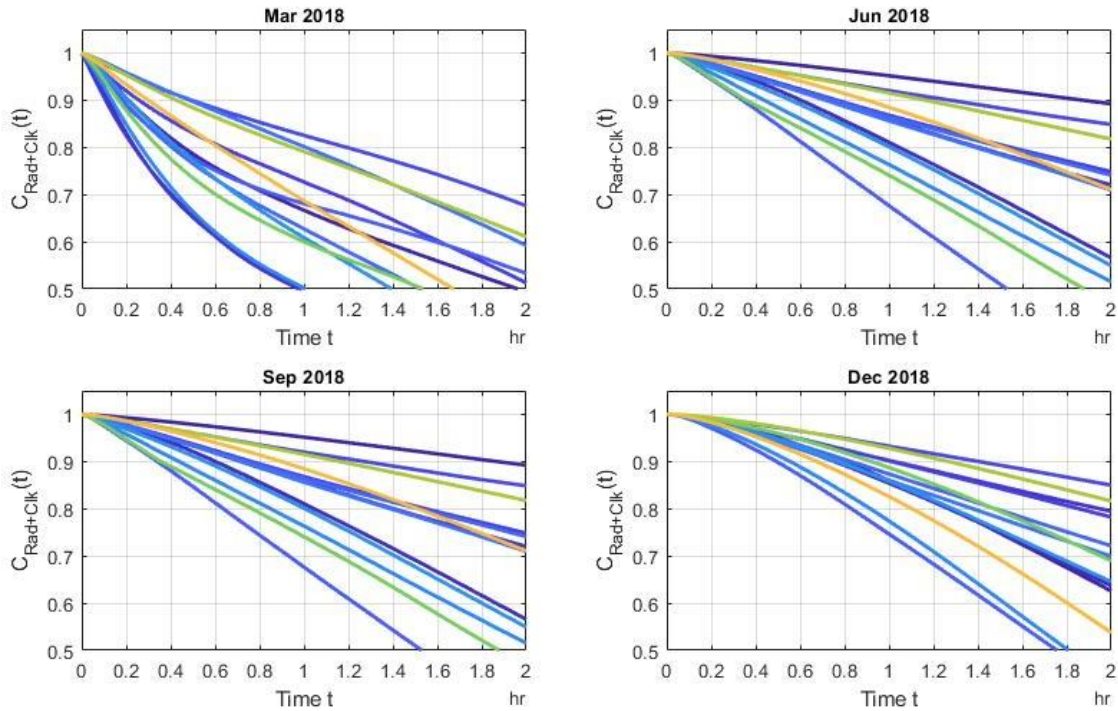


Figure 7: Season impact on orbit and clock errors stationarity of Galileo satellites

To understand if the spread observed here is due to solar impact or if it is due to the accuracy of our autocorrelation estimate, we generated 31 (i.e. number of GPS satellites) first order Gauss Markov Random Processes (with a sigma of 1 m) with a length of one month and computed their autocorrelations. In Figure 8, we represented the theoretical autocorrelations of GMRP (left) with respect to the autocorrelation of orbit and clock errors (right) for the month of December 2018. Since we are trying to model the orbit and clock errors as first order GMRP, we would expect the two figures to be similar. Additionally, the results on the left are consistent with the ones obtained in Figure 4. Therefore, it is not possible to determine whether the spread on the real data (right figure) is due to the sun or to the uncertainty on our autocorrelation estimate (left figure).

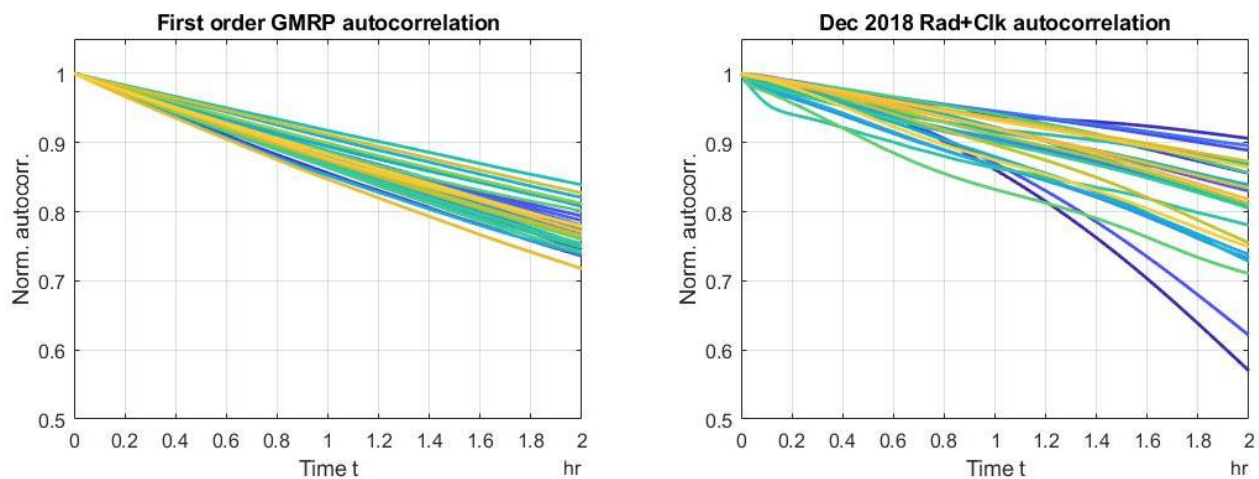


Figure 8: Theoretical (model) VS Real data orbit and clock error autocorrelations

In this section, we showed that the orbit and clock errors were stationary with respect to lunar cycle but that these same errors may be impacted by seasonal changes. This uncertainty in stationarity will need to be accounted for in the next section.

BOUNDING OF THE AUTOCORRELATION

To model orbit and clock errors in our batch ARAIM implementation, we need to account for their time correlation. The stationarity study conducted above concluded that orbit and clock errors may be impacted by seasonal changes. Given these observations, several options can be considered to account for correlation in our batch covariance matrix. A first option would be to bound the worst autocorrelation set (i.e. widest spread, i.e. all of the subplots in Figure 6). This method is the most conservative of the ones proposed here.

Since the behavior of the autocorrelation function (especially GPS) does not perfectly match a GMRP near zero, we chose to model the lower bound as the sum of autocorrelations of a White Gaussian Noise (WGN) and a GMRP as described in Equation (11). By doing so, the lower bound becomes tighter and less conservative.

$$\hat{C}_{XX_{LOWER}} = \epsilon\delta(0) + (1 - \epsilon)e^{-t/\tau} \tag{11}$$

Where

- ϵ is a small real value
- δ is the Dirac delta function (i.e. autocorrelation function of a WGN)
- τ is the time constant of the GMRP

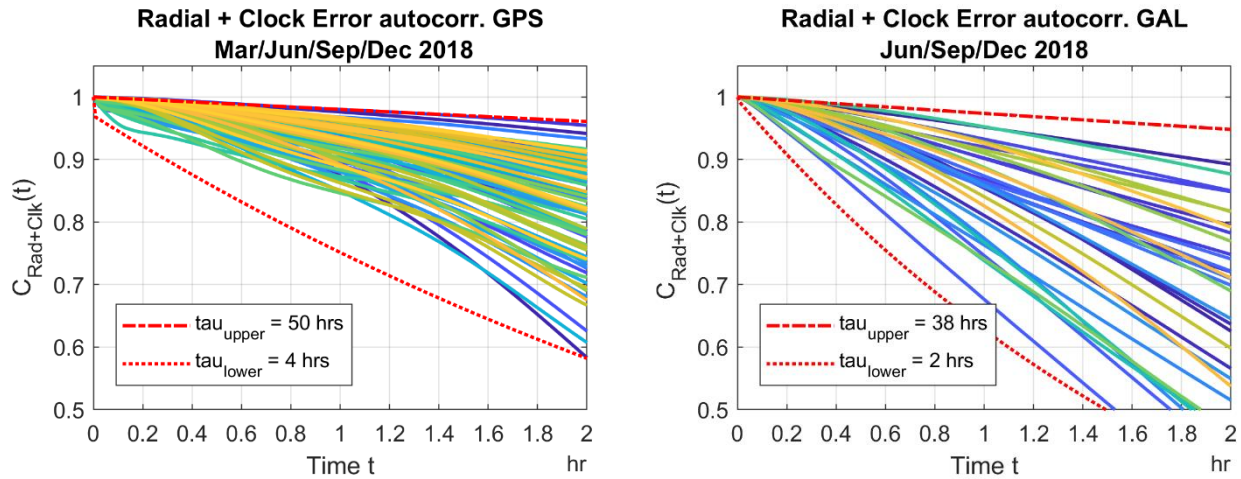


Figure 9: Example of autocorrelation bounding for GPS (left) and Galileo (right) satellites

Figure 9 represents the orbit and clock errors (i.e. radial-plus-clock) of each GPS (left) and Galileo (right) satellites, with data taken over the four (three, for Galileo) data sets shown in previous section (March, June, September, December 2018). Once again, the color code is as follows: each color represents one of the GPS satellite (31 in total), using one month of data, but zooming in on the first two hours. So the figure on the left will have 31*4 curves (31 satellites at 4 different months). In addition to that, the red curves represent the upper and lower bounds (first order GMRP) we obtained. GPS satellites are upper and lower bounded with GMRP of time constants 4 hours and 50 hours. Galileo satellites are bounded with GMRP of time constants 2 hours and 38 hours.

Another option would be to evaluate autocorrelation satellite by satellite. Figure 10 represents an example of bounding according to our second option. This time, each color represents a different month of data of the year 2018 for a given PRN (here PRN 07). GPS PRN 07 was bounded with GMRP of time constant 10 hours and 29 hours. Galileo PRN 12 was bounded with GMRP of time constant 2 hour and 13 hours. Modeling autocorrelation functions satellite-by-satellite has the advantage of providing tighter bounds, but at the cost of a more complex implementation.

One can note that the results in Figure 10 (left) have a similar spread as the theoretical autocorrelations represented in Figure 8 (right).

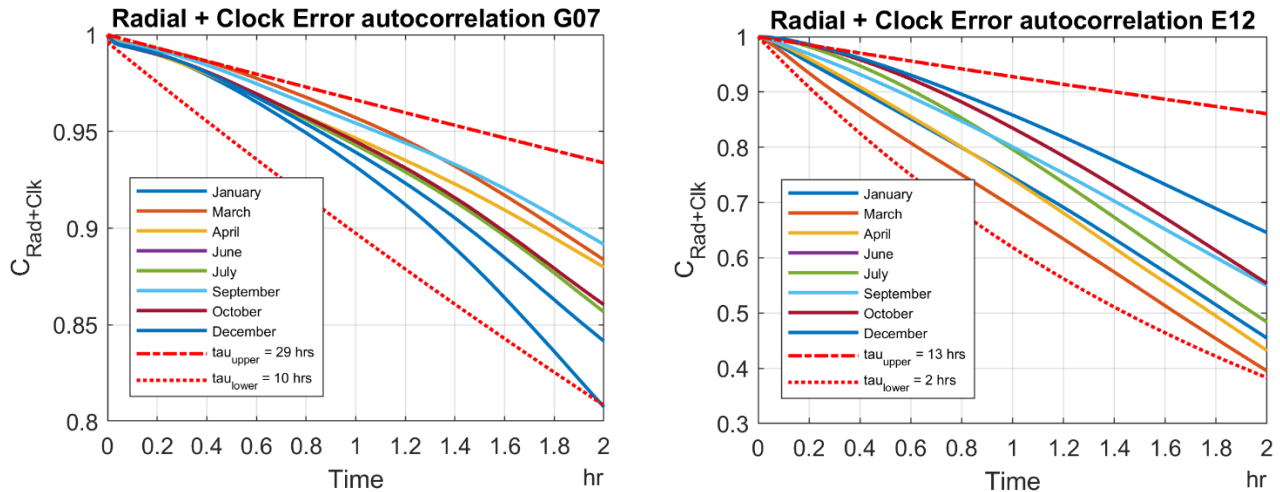


Figure 10: Example of satellite error calibration with GPS PRN 07 and Galileo PRN 12

In this section, we presented two options for upper and lower bounding of the orbit and clock errors autocorrelations. The first method has the advantage of being simple to implement in a batch, but at the expense of being conservative. The second method was less conservative but at the cost of a more complex implementation.

CONCLUSION

We analyzed months of orbit and clock error data to derive upper and lower bounds on their autocorrelation functions. First, we had to interpolate GPS orbit and clock ephemeris to obtain realistic autocorrelation functions, and we analyzed the impact of this interpolation process. Second, for data processing, two conflicting aspects had to be considered: on the one hand, the length of the data collection process needed to be large enough to provide an accurate autocorrelation function estimate, while on the other hand, it had to be limited to ensure the process would remain stationary. We evaluated the stationarity of GPS and Galileo orbit and clock error autocorrelation functions with respect to lunar cycles (28 days) and solar cycles (seasons). The seasonal analysis was inconclusive for both the GPS and Galileo constellations, and thus bounding was performed on the worst-season data set, using data collected in December.

Finally, the paper shows that orbit and clock error autocorrelation functions can be upper and lower bounded with Gauss Markov Process autocorrelation functions with time constants of 50 h and 4 h, respectively, for GPS and 38 h and 2 h, respectively, for Galileo. A less conservative option would be to derive these upper and lower bounds for each satellite individually. In the next step of this research, we will apply similar methods to other error sources (e.g. troposphere). Sequential ARAIM algorithms could then be implemented over longer durations, which would open the possibility to extend the scope of ARAIM applications beyond aircraft navigation, to rail, harbor or arctic navigation (open sky). Additionally, we will employ these models in the work of [6] which provides positioning integrity risk bounding capability using a Kalman filter framework.

ACKNOWLEDGMENTS

The authors would like to thank the Federal Aviation Administration (FAA) for their support of this research. However, the opinions in this paper are our own and do not necessarily represent those of any other person or organization.

REFERENCES

1. Joerger, M., Pervan, B., "Exploiting Satellite Motion in ARAIM: Measurement Error Model Refinement Using Experimental Data," *Proceedings of the 29th International Technical Meeting of the Satellite Division of The Institute of Navigation (ION GNSS+ 2016)*, Portland, Oregon, September 2016, pp. 1696-1712. <https://doi.org/10.33012/2016.14552>
2. Working Group C. "ARAIM Technical Subgroup. Interim Report Issue 1.0." Technical report, EU-US Cooperation on Satellite Navigation, 2012.

3. Working Group C. "ARAIM Technical Subgroup. Milestone 2.0 Report." Technical report, EU-US Cooperation on Satellite Navigation, 2014.
4. Working Group C. "ARAIM Technical Subgroup. Milestone 3.0 Report." Technical report, EU-US Cooperation on Satellite Navigation, 2016.
5. M. Joerger, L. Gratton, B. Pervan, and C. E. Cohen. "Analysis of Iridium-Augmented GPS for Floating Carrier Phase Positioning." *NAVIGATION: Journal of the Institute of Navigation*. 57.2. (2010): pp 137-160.
6. Langel, S., Khanafseh, S., Pervan, B., "Bounding Integrity Risk in the Presence of Parametric Time Correlation Uncertainty," *Proceedings of the 2012 International Technical Meeting of The Institute of Navigation*, Newport Beach, CA, January 2012, pp. 1666-1680.
7. Stanford University, "GPS Ephemeris Repository", [Online]. Available: <https://gps.stanford.edu/suglephemeris-files>.
8. Centre National d'Etudes Spatiales, CNES, "Broadcast ephemeris data repository." [Online]. Available: <ftp://serenad-public.cnes.fr/SERENAD0/FROM NTMFV2/NAV/>
9. International GNSS Service, "Data Repository" [Online]. Available: <ftp://cdis.gsfc.nasa.gov/gps/data/>
10. S. Perea, "Design of an Integrity Support Message for Offline Advanced RAIM", PhD Dissertation, May 2019.
11. S. E. Langel, "Bounding Estimation Integrity Risk for Linear Systems With Structured Stochastic Modeling Uncertainty", PhD Dissertation, May 2014.
12. J. S. Bendat, A. G. Piersol, "Random Data Analysis Measurement Procedure", 2nd Edition, pp. 271-273.
13. Radio Technical Commission for Aeronautics (RTCA) Special Committee 159, "Minimum Operational Performance Standards for Global Positioning System/Wide Area Augmentation System Airborne Equipment," 2009.
14. O. Montenbruck, P. Steigenberger, and A. Hauschild, "Broadcast versus precise ephemeris: a multi-GNSS perspective", *GPS Solutions*, June 2014.
15. M. Schenewerk, "A Brief Review of basic GPS Orbit Interpolation Strategies", *GPS Solutions*, vol. 6, no. 4, pp. 265{267, Mar 2003. [Online]. Available: <https://doi.org/10.1007/s10291-002-0036-0>

APPENDIX A: EPHEMERIDES INTERPOLATION

The GPS constellation broadcasts a new set of ephemerides every 2 hours. Each set of ephemerides is valid for 4 hours. Hence, when a new set of ephemerides is received after 2 hours, the previous one is still valid for another 2 hours. This paper has shown that the radial, along track, cross track orbit and clock errors were impacted by jumps due to the ephemerides update. The purpose of this paper is to propose a model for orbit and clock errors that would account for their correlation in time. The approach used here was to determine upper and lower bound of the orbit and clock error autocorrelations that could be modelled as a first order GMRP (i.e. continuous error model). Accounting for the jumps in our batch implementation, we would need to model the dynamic behavior of these jumps and input this model to our batch or KF algorithm. Since smoother dynamics are more convenient to model and since we want to model those errors as first order GMRP, we will use interpolated broadcast ephemerides in this work.

The current (X_{cur}) and next (X_{next}) set of ephemerides were interpolated in the position and velocity domain through weights over an interpolation window W_{Int} of 2 hours:

$$\hat{X}(i+j) = \frac{j}{W_{Int}} X_{next}(i+j) + \frac{W_{Int}-j}{W_{Int}} X_{cur}(i+j) \quad (A.1)$$

Where

- X_{cur} is the current set of ephemerides
- X_{next} is the next set of ephemerides
- \hat{X} is the (output) interpolated ephemerides
- W_{Int} is the two hours interpolation window
- i is the index of the jump
- j is a dummy variable such that $j \in \llbracket 0, W_{Int} \rrbracket$

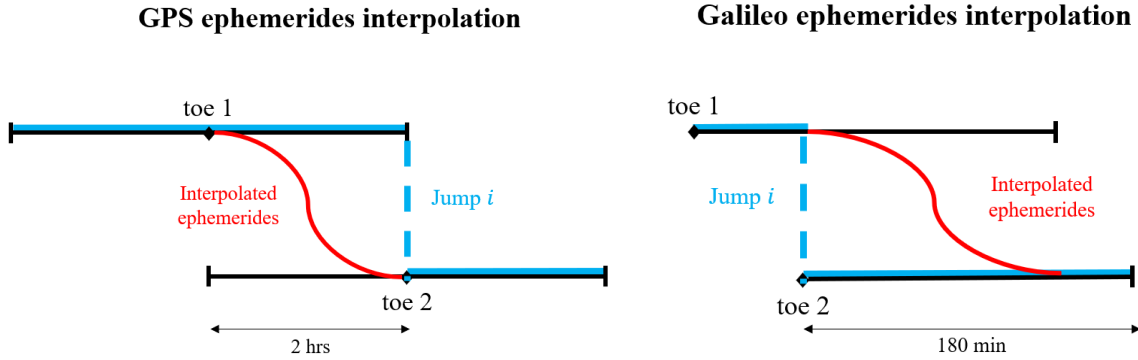


Figure 11: Ephemeris interpolation scheme for GPS (left) and Galileo (right)

Figure 11 represents the interpolation process for GPS and Galileo. Since Galileo's updates are different from GPS, the two interpolations are slightly different. GPS broadcast a new set of ephemerides every two hours, and each set is valid for a total of 4 hours. On the other hand, Galileo broadcast a new set of ephemerides every 8-12 minutes, and each set is valid for a total of 180 min. The interpolation process chosen for Galileo is similar to the one used for GPS, and uses Equation (A.1) with $W_{Int} = 180 * 60 - (t_{oe2} - t_{oe1})$, as seen in Figure 11.

APPENDIX B: VARIANCE OF NORMALIZED AUTOCORRELATION ESTIMATE

Let us define the autocorrelation estimate of a random process X as:

$$\hat{R}_{XX}(t) = R_{XX}(t) + \delta R_{XX}(t) \quad (\text{B.1})$$

Where

$R_{XX}(t)$ is known
 $\delta R_{XX}(t)$ is unknown

In this paper, we are interested in a normalized autocorrelation, as described in Equation (4). Substituting (B.1) into (13), we obtain:

$$\hat{C}_{XX}(t) = \frac{R_{XX}(t) + \delta R_{XX}(t)}{R_{XX}(0) + \delta R_{XX}(0)} \quad (\text{B.2})$$

Factorizing by $C_{XX}(t)$:

$$\hat{C}_{XX}(t) = C_{XX}(t) \left(\frac{1 + \delta R_{XX}(t)/R_{XX}(t)}{1 + \delta R_{XX}(0)/R_{XX}(0)} \right) \quad (\text{B.3})$$

Neglecting second order terms and given $\delta R_{XX}(0) \ll R_{XX}(0)$:

$$\hat{C}_{XX}(t) = C_{XX}(t) + \frac{\delta R_{XX}(t)}{R_{XX}(0)} - \frac{R_{XX}(t)}{R_{XX}(0)^2} \delta R_{XX}(0) \quad (\text{B.4})$$

Therefore, moving the first time in the right and side of Equation (B.4), the second moment is derived as:

$$\text{E} \left[\left(\hat{C}_{XX}(t) - C_{XX}(t) \right)^2 \right] = \frac{\sigma_{\hat{R}_{XX}(t)}^2}{R_{XX}(0)} - 2 \frac{R_{XX}(t)}{R_{XX}(0)^3} \text{E}[\delta R_{XX}(t) \cdot \delta R_{XX}(0)] + \frac{R_{XX}(t)^2}{R_{XX}(0)^4} \sigma_{\hat{R}_{XX}(0)}^2 \quad (\text{B.5})$$

We can note that the first and last terms of Equation (B.4) can be derived with Equations (15) and (16). Hence, the only unknown is the expectation term. Since this term cannot be derived, we will upper and lower bound it.